

## Preparation and Spectroscopic Characterization of Ilmenite-Type $\text{CoTiO}_3$ Nanoparticles

Guo-Wei Zhou,<sup>†</sup> Don Keun Lee, Young Hwan Kim, Chang Woo Kim, and Young Soo Kang<sup>\*</sup>

<sup>†</sup>School of Chemical Engineering, Shandong Institute of Light Industry, Jinan 250100, P. R. China  
Department of Chemistry, Pukyong National University, Busan 608-737, Korea. \*E-mail: yskang@pknu.ac.kr  
Received August 15, 2005

The cobalt titanate,  $\text{CoTiO}_3$  nanoparticles have been prepared by calcinations of precursor obtained from a mixture of  $\text{TiO}_2$  and  $\text{Co(OH)}_2$  in aqueous cetyltrimethylammonium bromide (CTAB) solution. The nanoparticles were investigated with X-ray powder diffraction (XRD), transmission electron microscopy (TEM), X-ray photoelectron spectroscopy (XPS) and thermogravimetric/differential thermal analysis (TGA/DTA) to determine the crystallite size and the phase composition. The spectroscopic characterizations of these nanoparticles were also done with UV-Vis spectroscopy and FT-Raman spectroscopy. XRD patterns show that  $\text{CoTiO}_3$  phase was formed at calcinations temperature above 600 °C. UV-Vis absorption spectra indicate that the  $\text{CoTiO}_3$  nanoparticles have significant red shift to the visible region (400-700 nm) with  $\lambda_{\text{max}} = 500$  nm compared to pure  $\text{TiO}_2$  powder ( $\lambda_{\text{max}} = 320$  nm). The new absorption peaks (absorption at 696, 604, 520, 478, 456, 383, 336, 267, 238, 208  $\text{cm}^{-1}$ ), which were not appeared in FT-Raman spectra of P-25, also confirm the formation of Ti-O-Co bonds at above 600 °C and just not the mixtures of titanium dioxide with cobalt oxides.

**Key Words :** Cobalt titanate  $\text{CoTiO}_3$ , Nanoparticles, CTAB micelle solution

### Introduction

The titanium dioxide ( $\text{TiO}_2$ ) powder (P-25), which is a standard material in the field of photocatalytic reactions, includes anatase and rutile phase. It has been widely investigated since it can be used in many important fields such as in the environmental photocatalytic degradation of organic compound in waste water,<sup>1-4</sup> and utilization of solar energy.<sup>5-11</sup> The effect of doping other transition metals is to change the equilibrium concentration of electrons or holes. It has been known that the advantage of the doping of the metal ions in  $\text{TiO}_2$  is the temporary trapping of the photo-generated charge carriers by the dopant and the inhibition of their recombination during migration from inside of the material to the surface or the enhanced association of the functionalized organic pollutants to the doping ion surface sites. The doping of transition metal ions may significantly influence the optical properties of  $\text{TiO}_2$  photocatalyst, and the light absorption band of M- $\text{TiO}_2$  can be shifted into the visible region.<sup>12-18</sup>

Ilmenite-type mixed oxides, such as  $\text{FeTiO}_3$  (ilmenite) and the iso-structural compound  $\text{CoTiO}_3$  can come from  $\text{ABO}_3$ , which is the corundum-type structure of  $\text{A}_2\text{O}_3$  sesquioxides when half of the A cations of a corundum-type sesquioxide are substituted by a B cation. Obviously, A and B cations can be both trivalent, or A divalent and B tetravalent (as in ilmenite-type titanates), or, finally, A monovalent and B pentavalent, respectively. There have been several papers on the applications of  $\text{TiO}_2$ -supported Co oxide investigated previously owing to their potential industrial applications as catalysts and catalyst supports in recent years,<sup>9,19,20</sup> but the synthesis and the characterization of ilmenite-type cobalt titanate in micelle solutions have not been reported so far.

In the present work, we report the synthesis and characterization of cobalt titanate,  $\text{CoTiO}_3$  nanoparticle produced by commercial titania powder (P-25) support with transition metal hydroxide in cetyltrimethylammonium bromide (CTAB) micelle template, followed by calcination. Here the CTAB has a role of microreactor for the suppression of particle size and shape control. The morphology was studied with TEM and the structure and physical properties of nanoparticles were investigated by XRD, XPS, TGA/DTA, UV-Vis and FT Raman spectroscopic techniques.

### Experimental Section

**Materials.** Titanium dioxide powder P-25 is predominantly anatase (70% anatase, 30% rutile), it was purchased from Degussa Co. (Germany) and was used without any further treatment. Cetyltrimethylammonium bromide (CTAB) and cobalt nitrate hexahydrate ( $\text{Co(NO}_3)_2 \cdot 6\text{H}_2\text{O}$ ) were purchased from Aldrich Chemical Co. and were used as received. House distilled de-ionized water was passed through a four-cartridge Barnsted Nanopure II purification train consisting of macropure treatment.

**Preparation of  $\text{CoTiO}_3$  nanoparticles.** In a typical synthesis, 0.01 mol  $\text{Co(NO}_3)_2 \cdot 6\text{H}_2\text{O}$  was dissolved into 30 ml distilled de-ionized water. After stirring for 30 minutes, an aqueous solutions of 0.02 mol NaOH in 10 mL distilled de-ionized water were added drop by drop with stirring, which reacts to produce precipitation of  $\text{Co(OH)}_2$ . Then 0.01 mol of P-25 powder was added to the above solution. An aqueous micelle solution of CTAB (0.01 mol CTAB in 30 mL distilled de-ionized water) was added to the mixed solution under magnetic stirring at 75 °C and the suspension was refluxed for 12 hours at 75 °C. The supernatant was then

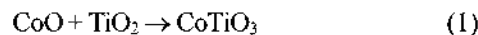
decanted, and the solid residue was washed three times with water. The as-synthesized solids were dried in air at 100 °C for 12 hours, ground to fine powder and calcined in air at 400, 500, 600, 700, 750, 800 and 900 °C for 6 hours, respectively.

**Characterization.** To investigate the phase composition and the crystallite size distribution of the nanoparticles after the calcinations, X-ray powder diffraction (XRD) measurements were performed. XRD was recorded on a Philips X'pert-MPD diffractometer in the  $2\theta$  range 20–80° using Cu K $\alpha$  radiation. The data were collected with a step of 0.02° ( $2\theta$ ) at room temperature. The chemical identity of the products was determined by comparing the experimental X-ray powder patterns to standards compiled by the Joint Committee on Powder Diffraction and Standards (JCPDS). The crystallite size was calculated from the peak widths using the Scherrer equation.

Transmission electron microscopy (TEM) studies were carried out with a JEOL JEM2010 transmission electron microscopy. The samples for TEM were ultrasonically dispersed in ethanol, and the suspension was deposited on a 400 mesh copper grid coated with a porous carbon film and then allowed to dry in air. X-ray photoelectron spectroscopy (XPS) studies were performed with a Vacuum Generators XPS (VG-Scientific ESCALAB 250 spectrometer) with monochromatized Al K $\alpha$  X-ray source (1486.6 eV). The C1s signal (285 eV) was taken as an internal standard to calculate the binding energies ( $E_b$ ). Thermogravimetric/differential thermal analysis (TGA/DTA) experiments were performed in air using a Perkin Elmer TGA7 Thermogravimetric Analyzer, from room temperature to 950 °C, with heating and cooling rate of 10 °C min<sup>-1</sup>. UV-Vis absorption spectra were obtained with a Varian Cary 1C UV-Visible spectrophotometer in the region 200–900 nm. FT-Raman spectra were recorded with a BRUKER (Germany) FRA-106/S spectrometer, using the 1064 nm excitation line of Nd-YAG Laser. The data were collected by keeping the power at 50 mW, 100 scans and 4 cm<sup>-1</sup> resolution.

## Results and Discussion

**Preparation of  $\text{CoTiO}_3$  nanoparticles.** Cetyltrimethylammonium bromide (CTAB) cationic surfactant was used as micellar template in water solutions. The concentration of CTAB controls the crystallite size of  $\text{Co}(\text{OH})_2$ .<sup>21</sup> When the calcination is done in air, some  $\text{Co}^{2+}$  ions present in  $\text{Co}(\text{OH})_2$  can be readily oxidized to  $\text{Co}^{3+}$  ions.<sup>22,23</sup> Those are the mixtures of  $\text{CoO}$ ,  $\text{Co}_2\text{O}_3$  or  $\text{Co}_3\text{O}_4$ . The  $\text{Co}(\text{OH})_2$  crystallites was oxidized in air in the presence of surfactant cylindrical micelle much more quickly than they do in the absence of surfactant because the smaller  $\text{Co}(\text{OH})_2$  particles react with oxygen faster and more completely.<sup>21</sup> The average oxidation state of  $\text{Co}(\text{OH})_2$  was changed from a majority of  $\text{Co}^{2+}$  to a majority  $\text{Co}^{3+}$  by calcinations. The surfactant template was removed and the  $\text{CoTiO}_3$  compounds must have been produced from reaction of titanium dioxide and cobalt oxides ( $\text{CoO}$  and  $\text{Co}_3\text{O}_4$ ) during calcination process<sup>19,24</sup>:



**XRD patterns.** In order to analyze the crystal phases, sizes and the formation temperature of  $\text{CoTiO}_3$ , X-ray diffraction (XRD) patterns were recorded. The obtained XRD patterns of samples at different calcination temperature are shown in Figure 1. All diffraction lines are well defined and compared to JCPDS card No. 78-1970, 77-1373, which indicate the presence of  $\text{Co}_3\text{O}_4$  and  $\text{CoTiO}_3$  in the products, respectively. The XRD peaks of powder calcined at 500 °C are very different from those of the samples at higher temperature 600, 700, 750 and 800 °C, which suggests that a significant formation of  $\text{CoTiO}_3$  at above 600 °C from reaction of  $\text{TiO}_2$  with  $\text{Co}_3\text{O}_4$  according to the equation (2). That is, above 600 °C most of the  $\text{TiO}_2$  and  $\text{Co}_3\text{O}_4$  particles react to form  $\text{CoTiO}_3$  compounds. The identified phases and the crystallite sizes of products with respect to calcinations temperature are shown in Table 1. The crystallite sizes of

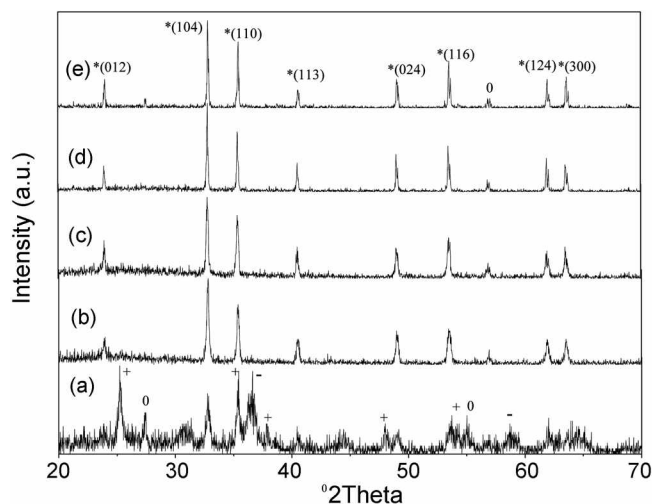


**Figure 1.** XRD patterns of as-synthesized particles calcined at various temperatures (a) 500 °C, (b) 600 °C, (c) 700 °C, (d) 750 °C, (e) 800 °C. Peaks corresponding to  $\text{CoTiO}_3$ ,  $\text{Co}_3\text{O}_4$ , anatase and rutile phase are marked by \*, +, - and 0, respectively.

**Table 1.** The phases and crystallite sizes of  $\text{Co}_3\text{O}_4$ ,  $\text{CoTiO}_3$  phases at different calcination temperatures

Calcination temperature (°C)	Phases	Crystallite size (nm)
500	$\text{Co}_3\text{O}_4$	$\text{Co}_3\text{O}_4$ (17)
	anatase, rutile	anatase (22)
600	$\text{CoTiO}_3$	24
	rutile	
700	$\text{CoTiO}_3$	38
	rutile	
750	$\text{CoTiO}_3$	49
	rutile	
800	$\text{CoTiO}_3$	62
	rutile	
900	$\text{CoTiO}_3$	73
	rutile	

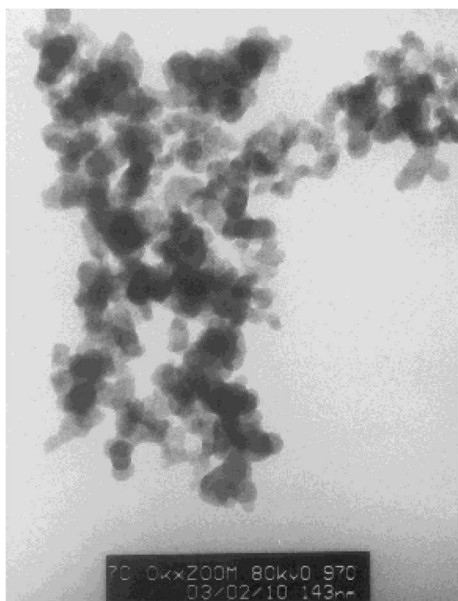


**Figure 2.** TEM images of CoTiO<sub>3</sub> sample calcined at 750 °C.

anatase and Co<sub>3</sub>O<sub>4</sub> were 22 and 17 nm at 500 °C; respectively, which is agreement with those in P-25 (anatase, 20 nm) and in the Co/TiO<sub>2</sub> results (Co<sub>3</sub>O<sub>4</sub>, 17.9 nm) reported by Brik *et al.*<sup>19</sup> It is shown that the crystallite sizes increase as the calcination temperature increases, but they are kept into the nanocrystalline range.

**TEM studies.** Transmission electron microscopic (TEM) observation of typical samples indicates the nanocrystalline nature of particles is almost spherical or slightly stretched. This is well shown in Figure 2. Rather dark crystalline spots can be observed beside less dark region. These dark spots and less dark spots can be assumed to be the different orientation of CoTiO<sub>3</sub> nanocrystallites, respectively, because the brightness and darkness of items in TEM image depends on its orientation. The nanoparticles size is between 40-70 nm, these are agree with the result of XRD.

**XPS results.** The core levels of transition elements present generally a main peak accompanied by an adjacent satellite (shoulder) located at higher binding energy ( $E_b$ ). The complicated processes involved (shake-up peaks) are often interpreted in terms of ligands  $\rightarrow$  metal charge transfers. In fact, in most cases, the spectral features allow the identification of the elements, the determination of their valence state and the concentration on a surface. The Co 2p and Ti 2p XPS spectra of CoTiO<sub>3</sub> at calcinations temperature 700 and 800 °C are shown in Figure 3(A) and (B), respectively, and the binding energy are listed in Table 2. The main signals of Co 2p<sub>3/2</sub> and Co 2p<sub>1/2</sub> doublet are separated by 15.9 and 16.1 eV in the calcination temperatures of 700 °C and 800 °C, respectively. The binding energy of Co 2p in pure CoO are as  $7E_b$  (Co 2p<sub>3/2</sub>) = 780.0 eV and  $E_b$  (Co 2p<sub>1/2</sub>) = 795.9 eV, respectively.<sup>24</sup> It can be concluded that the binding energy for Co 2p in CoTiO<sub>3</sub> shifted to lower energy compared with Co 2p in CoO and shifted to lower energy with the calcinations temperature increases. The slightly lower Co 2p binding energy might be

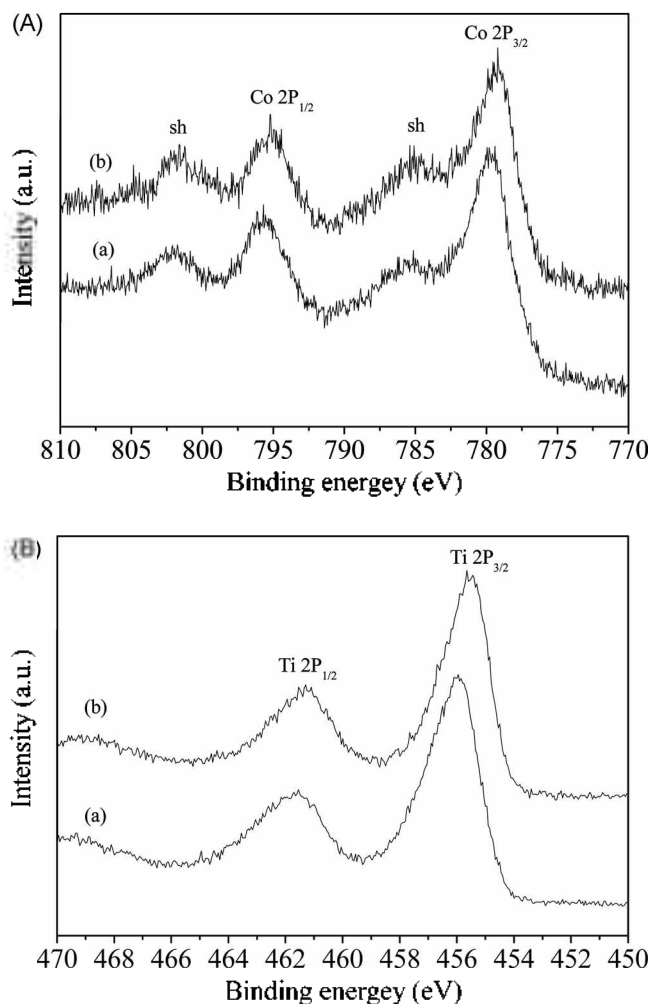


**Figure 3.** XPS spectra of Co 2p (A) and Ti 2p (B) in the CoTiO<sub>3</sub> sample calcined at (a) 700 and (b) 800 °C.

**Table 2.** Binding energy of CoTiO<sub>3</sub> at calcinations temperature 700 and 800 °C

calcinations temperature (°C)	$E_b$ (eV)		$\Delta E$ (eV)	$E_b$ (eV)		$\Delta E$ (eV)
	Co 2p <sub>3/2</sub>	Co 2p <sub>1/2</sub>		Ti 2p <sub>3/2</sub>	Ti 2p <sub>1/2</sub>	
700	779.8	795.7	15.9	456.2	461.6	5.4
800	779.2	795.3	16.1	455.6	461.2	5.6

explained by weakening of covalent nature of Co-O bond due to formation of Co-O-Ti bond. It also indicates a shoulder peak (sh) at their high-energy side. Such signals can only be observed with Co(+2) particles in the high spin state. The diamagnetic low spin Co<sup>3+</sup> ion does not show shake-up structures. The Co binding energies in CoO are  $E_b$  (Co 2p<sub>3/2</sub>) = 780.0 eV,  $E_b$  (Co 2p<sub>1/2</sub>) = 795.9 eV, and in Co<sub>3</sub>O<sub>4</sub> are  $E_b$  (Co 2p<sub>3/2</sub>) = 780.2 eV,  $E_b$  (Co 2p<sub>1/2</sub>) = 795.5 eV.<sup>24</sup> These are only slightly higher than those  $E_b$  in the CoTiO<sub>3</sub>. Therefore the XPS spectra of Co 2p point to the formation of Co-Ti-O bond.

It can also be find that the binding energy for Ti2p shifted to lower energy with the calcinations temperature increases.

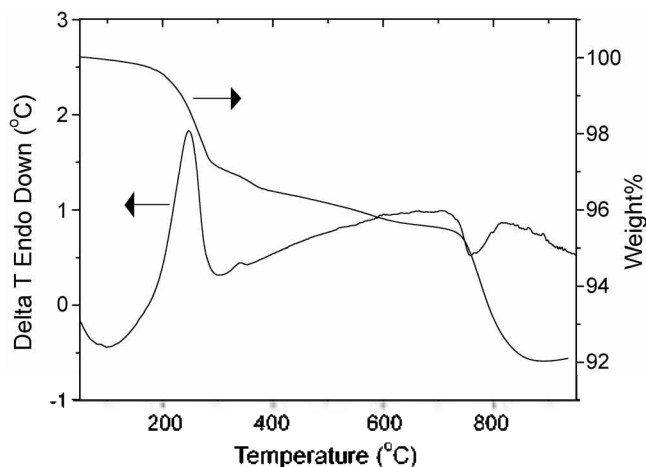


Figure 4. TGA/DTA curves of as-synthesized particles.

The main signals of the Ti  $2p_{3/2}$  and Ti  $2p_{1/2}$  doublet are separated by 5.4 and 5.6 eV in the calcinations temperatures of 700 °C and 800 °C, respectively. While a main doublet composed of two symmetric peaks situates at  $E_b$  (Ti  $2p_{3/2}$ ) = 458.4 eV,  $E_b$  (Ti  $2p_{1/2}$ ) = 464.0 eV in the spectrum of pure  $\text{TiO}_2$ .<sup>25</sup> The binding energy of Ti 2p shifted to lower energy indicates the formation of Co-Ti-O bond in our synthesized particles at 700 and 800 °C.

**Thermal analysis.** Thermogravimetric and differential thermal analysis (TGA/DTA) curves of as-synthesized sample are shown in Figure 4. The DTA curve shows two endothermic peaks at about 100 °C and 750 °C, and two exothermic peaks at about 250 °C and 340 °C. The simultaneously recorded TG curve shows a four step weight losses, the endothermic peaks and the exothermic peaks are associated to a weight loss. These can be interpreted in the following way. The first weight loss below 150 °C is due to the removal of water physically adsorbed on the as-synthesized surface. The second weight loss between 150 and 380 °C is attributed to the decomposition of surfactant CTAB that are trapped inside the matrix and also assigned to the removal of chemisorbed water. A third step of a small weight loss ranging from 380 to 700 °C may be due to the further removal of CTAB. An additional weight loss occurs in the range of 700-900 °C, this could be assigned to the oxygen removal during the formation of  $\text{CoTiO}_3$  on the support of  $\text{TiO}_2$  and  $\text{Co}_3\text{O}_4$  just like the above equations (2).<sup>19,24</sup> DTA curve presented in Figure 4 shows a corresponding exothermic peak at 250 and 340 °C. This supports the CTAB decomposition. The endothermic peak at about 750 °C supports the formation of cobalt titanate  $\text{CoTiO}_3$ .

**UV-Visible spectra.** UV-Vis spectra for as-synthesized particles at different calcinations temperatures are shown in Figure 5. The UV-vis spectra of as-synthesized powder at lower temperature (400 and 500 °C) can be characterized by an absorption band at the wavelength of 250-320 nm as shown in Figure 5(a) and (b), these just like the absorbance of pure P-25 powder.<sup>9,20</sup> This indicates the as-synthesized powder is just the mixture of P-25 and cobalt oxide not the formation of cobalt titanate. The strong absorption in the UV

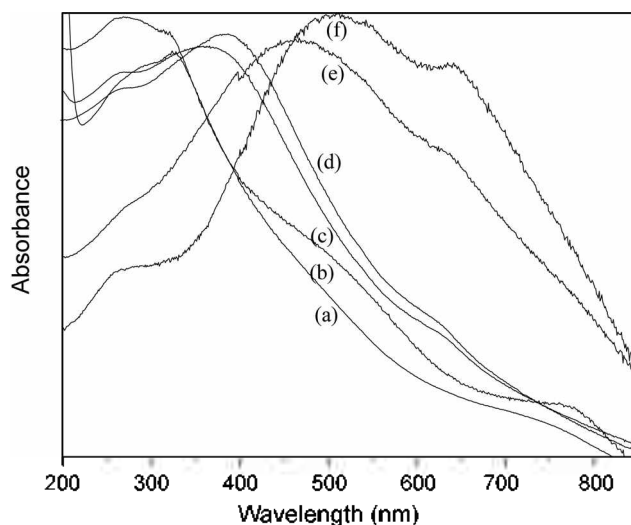


Figure 5. UV-Vis absorption spectra of as-synthesized particles at different calcination temperatures (a) 400 °C, (b) 500 °C, (c) 600 °C, (d) 700 °C, (e) 750 °C and (f) 800 °C.

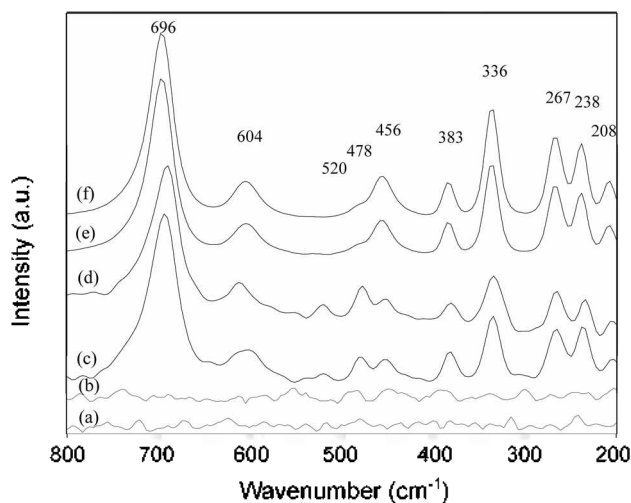


Figure 6. FT-Raman spectra of as-synthesized particles at different calcination temperatures at (a) 400 °C, (b) 500 °C, (c) 600 °C, (d) 700 °C, (e) 750 °C, (f) 800 °C.

range is due to  $\text{TiO}_2$  powder inter-band transitions (valence band  $\rightarrow$  conduction band). The  $\lambda_{\text{max}}$  appearing at 320 nm is related to  $\text{O}^{2-} \rightarrow \text{Ti}^{4+}$  charge transfer transitions. The UV-vis spectra of the as-synthesized compound at higher temperature as shown in Figure 5(c)  $\rightarrow$  (d) reveal a wide absorption bands at the visible region wavelength of 400-700 nm, with  $\lambda_{\text{max}}$  at 410 nm (600 and 700 °C) and  $\lambda_{\text{max}}$  at 500 nm (750 and 800 °C). These are already reported that it indicates the formation of tetrahedral  $\text{Co}^{2+}$  species.<sup>26,27</sup> The bands located at 500-700 nm are associated with  $n_2$  absorptions that result from the transitions  ${}^4A_2(\text{F}) \rightarrow {}^4T_1(\text{F})$  and  ${}^4A_2(\text{F}) \rightarrow {}^4T_1(\text{P})$ . These transitions often split into three components because of the degeneracy lift of the excited levels  ${}^4T_1(\text{P})$  and  ${}^4T_1(\text{F})$  by spin-orbit coupling and the Jahn-Teller effect.<sup>26,27</sup> Moreover in the wavelength of 400-500 nm, contribution of octahedral  $\text{Co}^{2+} \rightarrow \text{Ti}^{4+}$  inter-valence charge transfer can be

involved.<sup>9</sup>

**FT Raman spectroscopy.** In recent years FT-Raman spectroscopy has become an increasingly valuable tool for the investigation of the supported catalysts.<sup>9,19,28,29</sup> The spectra of as-synthesized particles at different temperature are comparatively shown in Figure 6. Titanium dioxide is characterized by anatase (three bands at 397, 516 and 639  $\text{cm}^{-1}$ ) and rutile (one band at 447  $\text{cm}^{-1}$ ) according to the literature.<sup>9,19,28</sup> In the formation of  $\text{CoTiO}_3$  during the calcinations at above 600 °C, these four bands disappear and give rise to an extremely strong feature near 700  $\text{cm}^{-1}$ , which is certainly due to a true vibrational peak. There is no absorbance peak in the test range at lower temperature (400 and 500 °C), due to the as-synthesized compound mainly contain  $\text{TiO}_2$  and  $\text{Co}_3\text{O}_4$ .

According to the presence of a center of symmetry and the "mutual exclusion rule", Raman active bands are not expected. In the case of the formation of  $\text{CoTiO}_3$  particles, the center of symmetry is retained, so the mutual exclusion principle is still valid. In this case there should be ten Raman active modes ( $5 A_g + 5 E_g$ ).<sup>30</sup> Our results of ten Raman active fundamentals (absorption at 696, 604, 520, 478, 456, 383, 336, 267, 238 208  $\text{cm}^{-1}$ ) are consistent with the theoretical analysis. The most typical feature is the strong Raman mode observed near 700  $\text{cm}^{-1}$  on  $\text{CoTiO}_3$ . This mode arises from the highest frequency vibrational mode of  $\text{CoO}_6$  octahedra that is the symmetric stretching mode ( $A_{1g}$  symmetry for regular  $\text{O}_h$  octahedral). The phonon modes below 300  $\text{cm}^{-1}$  are assigned to lattice vibrations.<sup>9,30</sup> These results also indicate the formation  $\text{CoTiO}_3$  at above 600 °C and just not the mixture of  $\text{TiO}_2$  with cobalt oxide.

### Conclusion

The nanoparticles of  $\text{CoTiO}_3$  were prepared by the reaction of  $\text{TiO}_2$  powders (P-25) with transition metal hydroxide in CTAB micelle solutions and followed by calcination. The structural, chemical and light absorption properties of these particles were studied with TEM, XRD, XPS, TGA/DTA, UV-Vis and FT-Raman. XRD patterns show that  $\text{CoTiO}_3$  phase was formed at calcination temperatures above 600 °C. The prepared cobalt titanate at calcination temperatures above 600 °C show a significant absorption band shift into the visible region of 400-700 nm compared to pure of  $\text{TiO}_2$  powder. The new FT-Raman absorption peaks at 696, 604, 520, 478, 456, 383, 336, 267, 238, 208  $\text{cm}^{-1}$  for as-synthesized particles compared to P-25 also show the formation of Ti-O-Co bonds and just not the mixtures of titanium dioxide with transition metals at calcinations temperature above 600 °C. These materials are going to be tested for photodegradation of organic compounds in another work.

**Acknowledgement.** This work is financially supported by the Functional Chemicals Development Program in 2004-2005 and the Brain Busan 21 Project in 2004.

### References

- Ohno, T.; Sarukawa, K.; Tokieda, K.; Matsumura, M. *J. Catal.* **2001**, *203*, 82.
- Arslan, L.; Balcioglu, L.A.; Bahnmann, D.W. *Appl. Catal. B Environ.* **2000**, *26*, 193.
- Zhang, Q.; Gato, L.; Guo, J. *Appl. Catal. B Environ.* **2000**, *26*, 207.
- Taguchi, J.; Okura, T. *Appl. Catal. A Gen.* **2000**, *194/195*, 789.
- Takaca, T.; Furumi, Y.; Shinohara, K.; Tanaka, A.; Hara, M.; Kondo, J. N.; Domen, K. *Chem. Mater.* **1997**, *9*, 1063.
- Fujihara, K.; Ohno, T.; Matsumura, M. *J. Chem. Soc. Faraday Trans* **1998**, *94*, 3705.
- Ohno, T.; Haga, D.; Fujihara, K.; Kaizaki, K.; Matsumura, M. *J. Phys. Chem. B* **1997**, *101*, 6415.
- Sayama, K.; Arakawa, H. *J. Phys. Chem.* **1993**, *97*, 531.
- Brik, Y.; Kacimi, M.; Ziyad, M.; Francois, B. V. *J. Catal.* **2001**, *202*, 118.
- Stranick, M. A.; Houalla, M.; Hercules, D. M. *J. Catal.* **1987**, *106*, 362.
- Jeźlorowski, H.; Knozinger, K.; Grange, P.; Gajardo, P. *J. Phys. Chem.* **1980**, *84*, 1825.
- Koerts, T.; Vansanten, R. A. *J. Chem. Soc. Chem. Comm.* **1991**, 1281.
- Pareja, P.; Amariglio, A.; Belgued, M.; Amariglio, H. *Catal. Today* **1994**, *21*, 423.
- Noronha, F. B.; Perez, C. A.; Schmal, M.; Frety, R. *Phys. Chem. Chem. Phys.* **1999**, *1*, 2861.
- Okamoto, Y.; Nagata, K.; Adachi, T.; Inamura, K.; Takyu, T. *J. Phys. Chem.* **1991**, *95*, 310.
- Verberckmoes, A.; Weckhuysen, B. M.; Schoonheydt, R. A. *Micropor. Mesopor. Mater.* **1998**, *22*, 165.
- Yin, J. B.; Zhou, X. P. *Chem. Mater.* **2002**, *14*, 4633.
- Komoda, Y.; Sakai, N.; Rao, T. N. *Langmuir* **1998**, *14*, 1081.
- Brik, Y.; Kacimi, M.; Francois, B. V.; Ziyad, M. *J. Catal.* **2002**, *211*, 470.
- Dvoranova, D.; Brezova, V.; Mazur, M.; Malati, M. A. *Appl. Catal. B Environ.* **2002**, *37*, 91.
- Tian, Z. R.; Tong, W.; Wang, J. Y.; Duan, N. G.; Krishnan, V. V.; Suib, S. L. *Science* **1997**, *276*, 926.
- Shen, Y. F.; Suib, S. L.; O'Young, C. L. *J. Am. Chem. Soc.* **1994**, *116*, 11020.
- Cao, H.; Suib, S. L. *J. Am. Chem. Soc.* **1994**, *116*, 5334.
- Vob, M.; Borgmann, D.; Wedler, G. *J. Catal.* **2002**, *212*, 10.
- Pouilleau, J.; Devilliers, D.; Groult, H.; Marcus, P. *J. Mater. Sci.* **1997**, *32*, 5645.
- Verberckmoes, A.; Weckhuysen, B. M.; Schoonheydt, R. A. *Micropor. Mesopor. Mater.* **1998**, *22*, 165.
- Carter, R. L. *Molecular Symmetry and Group Theory*; John Wiley & Sons, Inc.: 1998; Chapter 7, p 201.
- Gotic, M.; Ivanda, M.; Popovic, S.; Music, S.; Sekulic, A.; Turkovic, A.; Furic, K. *J. Raman Spectrosc.* **1997**, *28*, 555.
- Choi, H. C.; Jung, Y. M.; Kim, S. B. *Bull. Korean Chem. Soc.* **2004**, *25*, 426.
- Baraton, M. I.; Busca, G.; Prieto, M. C.; Ricchiardi, G.; Escribano, V. S. *J. Solid State Chem.* **1994**, *112*, 9.